Feasibility of Multiple Excited-State Proton Transfer Processes in Hydroxyquinoline-containing Benzobisimidazole Dyes

Tatiana Munteanu, Dancho Yordanov, Gabriel Canard, Olivier Siri, Denis Jacquemin, Anton Georgiev, Simon Pascal

Feasibility of Multiple Excited-State Proton Transfer Processes in Hydroxyquinoline-containing Benzobisimidazole Dyes

Tatiana Munteanu,[a] Dancho Yordanov,[b,c] Gabriel Canard,[a] Olivier Siri,*[a] Denis Jacquemin,*[d,e] Anton Georgiev*[c] and Simon Pascal*[a,d]

Two new benzobisimidazole platforms incorporating 7-hydroxyquinoline moieties were synthesized and characterized to explore potential multiple proton transfer processes. Combining experimental analysis with theoretical insights, we investigated the photophysical properties and excited-state proton transfer phenomena within these systems and found that double proton transfer is unlikely to happen.

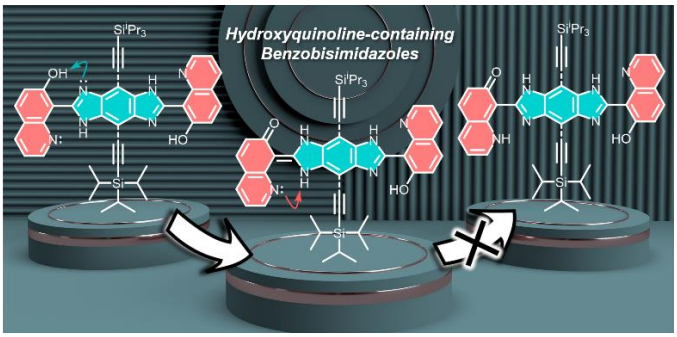

Introduction

Intra- and intermolecular hydrogen bonds hold pivotal roles in biological processes,[1–3] biopolymers,[4,5] molecular assemblies[6–8] as well as molecular architectures by, *e.g.*, enabling enol/keto tautomerization.[9–12] Excited-state intramolecular proton transfer (ESIPT) is a phototautomerisation process of organic molecules that can generate highly tuneable fluorescence covering all the visible spectral region (Figure 1).[11,13] The excited-state enol-to-keto proton transfer induces a significant structural change, resulting in a large Stokes shift between the keto emission and the enol absorption.[14–16] In addition, ESIPT molecules inherently undergo a significant π-electron rearrangement due to the interplay of the proton-donor and proton-acceptor sites,[17] making them sensitive to environmental factors such as solvent polarity,[18,19] pH,[20,21] metal ions,[22–24] aggregation,[25,26] and solid-state interactions.[1,27,28] They have found a wide range of applications in photonic and biomedical technologies, including OLEDs,[29–31] light amplification,[32] optical information storage,[33] fluorescent probes,[20,21,34–36] and cell imaging.[14,37]

Excited-state double proton transfer (ESDPT) constitutes an even more interesting phenomenon because two protons can be translocated within the same molecular structure, either by a synchronous or asynchronous mechanism.[38–47] As an example, a simple compound such as [2,2′-bipyridyl]-3,3′-diol shows photoexcited double proton transfer with emission bands at 510 and 568 nm related to the diketo and monoketo forms.[39,48] Experimental and theoretical studies indicated that the most likely mechanism is a sequential proton transfer.[39] Likewise, investigation on bisbenzoxazol-thiophene-diol dyes have pointed out the emergence of triple emission in the visible range due to the locally excited bis-enol form, the ESIPT keto-enol tautomer and the ESDPT bis-keto tautomer.[40,45] The ESDPT phenomenon can be exploited in applications such as laser dyes, living cell probes, and solar energy collectors. Multiple proton transfers are also sometimes assisted by surrounding solvent molecules.[42,43] A typical example is the assembly of 7-hydroxyquinoline in water or alcohol with indirect proton transport through an intermolecular solute-solvent hydrogen bonding bridge.[49–51] Since 7-hydroxyquinoline contains both proton-donor and proton-acceptor sites *via* the quinoline nitrogen, its substitution at the 8th position by suitable proton-acceptor-donor groups provides an opportunity to design an architecture that can undergo ESDPT (Figure 2). In this

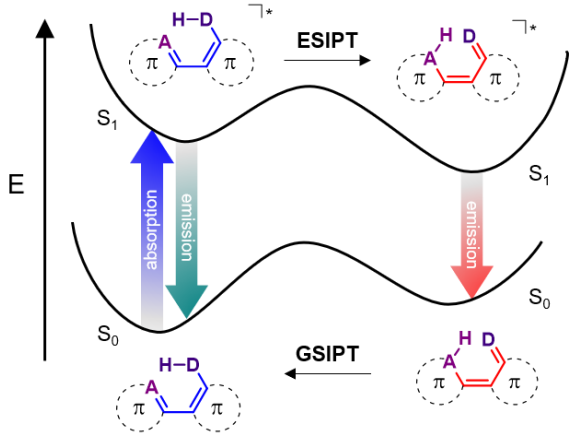

Figure 1. Illustration of the four-level phototautomerization process of excited-state and ground-state intramolecular proton transfers *(i.e.*, ESIPT and GSIPT) between the H-donor and H-acceptor sites (*i.e.*, D and A).

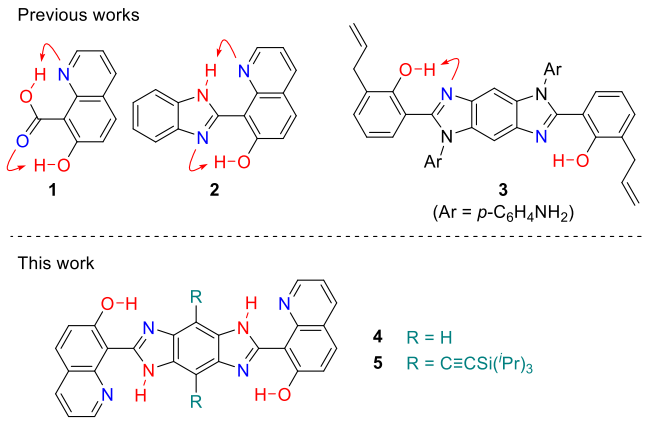

Figure 2. Top: previously studied 7-hydroxyquinoline-based (**1**,**2**) and BBI-based (**3**) compounds. Bottom: benzobisimidazole-hydroxyquinoline dyes (**4**,**5**) studied herein.

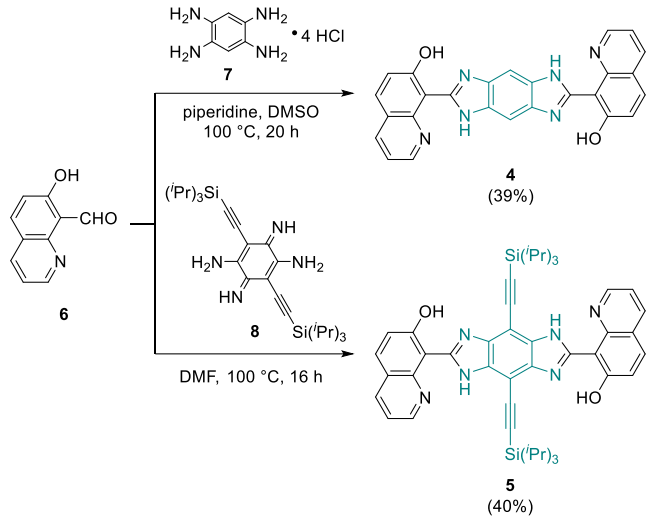

Scheme 1. Synthesis of BBI derivatives **4** and **5**.

framework, 7-hydroxyquinoline-8-carboxylic acid **1**[52,53] and 7-hydroxyquinoline-8-benzimidazole **2**[54] have been recently studied theoretically and experimentally. Notably, **2** shows a dual proton transfer due to structural asymmetry, affording a high energy emission band at *ca.* 420 nm ascribed to ESIPT and a low energy emission band at *ca.* 570 nm associated with the ESDPT process.

Given this background, we decided to progress one step further by incorporating two 7-hydroxyquinoline moieties on a benzobisimidazole (BBI) to potentially redshift the emission associated with the ESDPT and investigate the possible multiple proton transfer processes. BBI is a convenient ditopic platform that has been already investigated for generating ESIPT. Indeed, compound **3** (Figure 2), containing two 2-hydroxyphenyl units, was reported by Gryko and co-workers and features emission at 506 nm with a large Stokes shift of 6480 cm^{-1}, a relatively large fluorescence quantum yield and a good two-photon brightness.[55] Herein, we propose an investigation of two novel benzobisimidazole systems introducing 7-hydroxyquinoline: the BBI **4** with unsubstituted benzenetetramine core and the BBI **5** introducing (triisopropylsilyl)ethynyl moieties to improve its solubility (Figure 2). The experimental optical results were rationalized with the help of *ab initio* calculations that allowed to identify and discuss all the possible multiple proton transfers within both systems.

Results and discussion

The preparation of the BBI derivatives was envisaged *via* a conventional double condensation process involving two equivalents of 7-hydroxyquinoline-8-carbaldehyde (**6**) with tetraaminobenzene tetrahydrochloride (**7**) or TIPS-ethynyl-substituted diaminobenzoquinone diamine (**8**), as depicted in Scheme 1. Initial attempts in ethanol resulted in mixtures of partially condensed products that were challenging to separate. This outcome was attributed to the low solubility of both the starting materials and the intermediates in this solvent. Utilizing polar aprotic solvents, such as *N*,*N*-dimethylformamide (DMF) or dimethylsulfoxide (DMSO) at 100 °C, the symmetrical **4** and **5** dyes were obtained with respective yields of 39% and 40%, following simple purifications by precipitation or Soxhlet extraction. The identification of the BBI derivatives was confirmed by high-resolution mass spectrometry and their purity was assessed by NMR and infrared spectroscopies (see the ESI†).

The ^{1}H NMR spectra of **4** and **5** were acquired in different solvents, DMSO-d_6 and $CDCl_3$, respectively, for solubility reasons. In the 7.4–9.2 ppm range, both spectra display the anticipated six or five aromatic protons, respectively. However, no signals were detected for the OH and NH protons originating from the hydroxyquinoline and imidazole moieties in both compounds. This absence of signals is attributed to the inherent strong lability of these protons. Alternatively, the improved solubility of **5** allowed the acquisition of a ^{1}H NMR spectra in THF-d_8, which confirms the presence of the aromatic protons in the 9.0–7.5 ppm range, with the appearance of an additional signal at 14.0 ppm, assigned to two exchangeable protons (Figure S5, ESI†).

The absorption and emission spectra of the two BBI dyes are presented in Figure 3, whereas Table 1 compiles key photophysical data. In DMSO, the electronic absorption spectrum of **4** reveals two vibronic maxima at 394 and 415 nm, accompanied by molar extinction coefficients (ε) of *ca.* 34000 $M^{-1}cm^{-1}$. The incorporation of ethynyl-TIPS substituents in **5** induces moderate bathochromic and hyperchromic shifts of the absorption in DCM: two maxima are observed at 410 and 434 nm, with ε values of 57000 and 67000 $M^{-1}cm^{-1}$, respectively. To investigate the effect of the central ethynyl-TIPS function, the oxidation of **4** and **5** was assessed through electrochemical measurements (Figure S11, ESI†). Differential pulse voltammetry unveiled irreversible processes occurring at 0.96 V *vs.* SCE for **4** and 1.29 V for **5**, indicating a more difficult oxidation of the species possessing the ethynyl-TIPS function.

Regarding the emission properties, **4** presents a structured emission band centred at 443 nm and characterized by a rather small Stokes shift of 1410 cm^{-1}, apparently hinting at the absence of ESIPT. The excitation spectrum reproduces the absorption profile (see Figure S12, ESI†). It is noteworthy that

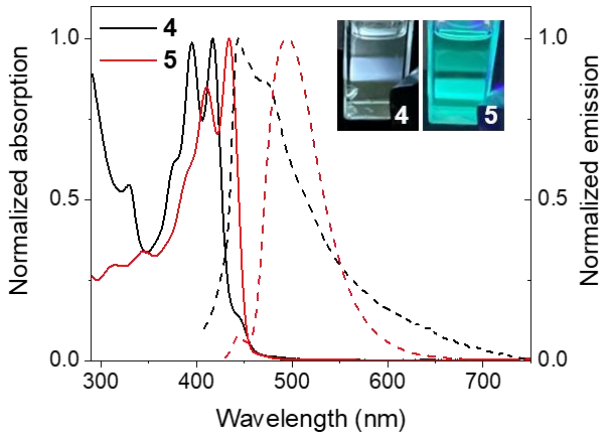

Figure 3. Normalized electronic absorption (plain lines) and emission (dashed lines) spectra of **4** in DMSO (black) and **5** in DCM (red). The pictures show the fluorescence of both compounds upon excitation at *ca.* 360 nm.

Table 1. Photophysical properties of **4** and **5**.

Dye	Conditions	λ_{abs} / nm (ε / $M^{-1}.cm^{-1}$)	λ_{em} / nm	Φ / %	τ / ns
4	DMSO	417 (34200), 395 (33800), 330 (18600)	443	0.1[a]	@435 nm: 0.8 (42%), 3.1 (42%), 10.2 (16%)
	solid	410, 335, 261	-	-	-
5	DCM	434 (66800), 410 (56700), 345 (22700)	495	2.5[b]	@495 nm: 0.12
	solid	429, 462	590, 639, 684	21[b]	@590 nm: 1.00 (41%), 2.75 (56%), 5.52 (3%) @639 nm: 0.95 (30%), 2.92 (67%), 6.3 (3%)

[a] Φ recorded with excitation at 363 nm, using anthracene as reference (Φ = 28% in ethanol). [b] Φ recorded using integration sphere.

this band is hypsochromically shifted compared to the references benzimidazole **2** (λ_{em} = 570 nm) and BBI **3** (λ_{em} = 506 nm).[54,55] The emission of **4** is characterized by a full width at half maximum (FWHM) of 3570 cm^{-1} and has a low fluorescence quantum yield below 1%. In contrast, **5** exhibits a narrow structureless fluorescence band peaking at 495 nm, characterized by a FWHM of 2420 cm^{-1}, a larger Stokes shift of 2840 cm^{-1} and a somewhat higher quantum yield of 2.5%. The different emission energies, Stokes shifts and width of the emission band let presume that the excited state processes might differ in **4** and **5** and may yield emissions occurring from different species (see also discussion below).

The optical properties of **4** could not be compared in different solvents due to solubility limitations. Nevertheless, the enhanced solubility of **5** enabled the examination of its solvatochromism in a large panel of solvents with varying polarities (Figure S14, ESI†). In general, the chromophore displayed limited solvatochromism, with two absorption maxima predominantly centred *ca*. 430–440 and 410 nm. Different behaviours were however obtained in both acetonitrile and methanol, where the compound exhibited significantly reduced solubility, resulting in redshifted absorption peaks at *ca.* 460 and 430 nm, with a broad shoulder on the low-energy side, presumably due to the presence of aggregation in the solution. Surprisingly, the emission spectra in these two polar solvents, and to a lesser extent in DMSO, show several maxima centred at 587, 623, and 680 nm that were attributed to aggregation of the compound in these solvents. This intriguing observation prompted us to delve into the solid-state absorption and emission of **5** (Figures S15 and S16, ESI†). As a powder, the absorption maximum of **5** is located at 462 nm, whereas a broad and structured emission spanning the 490–750 nm range is observed, characterised by two intense maxima at 590 and 639 nm with relatively high quantum yield of 21%. The solid-state emission spectra reproduced quite accurately the bands observed in polar media, *i.e.,* MeOH, MeCN and DMSO, confirming the aggregation of **5** in these solvents. The solid-state emission lifetime measurements show a triple exponential decay, indicating several contributions to the emission possibly arising from different aggregated forms of the compound at the solid state (Table 1 and Figure S16, ESI†). In contrast, **4** does not display solid-state emission, likely because aggregation is stronger, leading to fluorescence quenching. This indicates that the bulky ethynyl-TIPS moieties in **5** are efficient to enable solid-state emission by preventing intermolecular π-π stacking.

To gain further insights into a potential ongoing ESIPT processes, the optical properties of **5** were investigated at both 298 and 77 K in 2-methyltetrahydrofuran (Figure S17, ESI†). The emission spectra at both 298 and 77 K show comparable maxima centred at 492 and 488 nm, respectively, and only differ by a noticeable narrowing of the band (FWHM going from 2300 cm^{-1} at 298 K to 1430 cm^{-1} at 77 K). The Stokes shifts are also comparable, *ca*. 2500 cm^{-1}, indicating that the emission may exclusively arise either from the locally excited state or from a tautomer of close energy.

To help rationalizing the experimental outcomes, we have used theoretical chemistry, with methods detailed in the ESI†. For the ground-state of **4** the canonical structure as represented in Scheme 1 is logically found more stable than any possible tautomer (by at least 3.6 $kcal.mol^{-1}$). The absorption to the lowest excited state is bright and has a clear π-π* character. The second transition is dark and upshifted by *ca.* 0.4 eV, so there is no doubt on the absorbing state. The electron density difference (EDD) plot for the lowest transition can be found in Figure 4. We have chosen this representation for the excited states since several molecular orbital pairs contribute to the transition. EDD advantageously allows a single figure representation in such case. On the EDD, one notes that the lowest excited state is highly delocalized, with a slight decrease of density on the two hydroxyl groups, which is favourable to induce ESIPT since photoexcitation induces an increase of acidity.[56] However, this qualitative representation shows that this change of density is rather modest as compared to standard ESIPT dyes, a typical outcome for highly delocalized systems.[57]

We have next explored various possibilities for ESIPT in **4**. First, we recall that ESIPT is a thermodynamically-driven process,[58] *i.e.*, that proton transfer barriers are easily crossed,

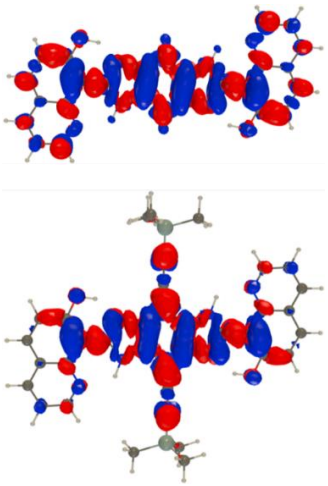

Figure 4. Electron density difference plots for the absorption of **4** (top) and **5** (bottom). The blue and red lobes represent regions of decrease and increase of density upon photon absorption. Level of theory: PCM-TD-TD-M06-2X/6-311+G(2d,p). Contour threshold: 0.0006.

and that the experimental outcomes are guided by the relative energies of the tautomers. In this context, we have determined the relative excited-state Gibbs free energies of many possible tautomers. Only the lowest excited state was considered, since the second state is at least 0.5 eV higher for all key structures, without indication of crossing or significant mixing, even at the transition state, *i.e.*, the nature of the excited state is essentially preserved during ESIPT. We also underline that there are always two intramolecular H-bonds between the core and each side groups, hampering large amplitude motions such as twisting. Key results are summarized in Figure 5 and S17 in the ESI†.

Starting from the canonical EE* form, transferring one proton yields an almost isoenergetic structure, whether the transfer involves the phenol or imidazole proton. Indeed, theory provides a ΔG of +0.01 eV, a negligible difference given the theoretical error bar. While both EE* and KE^{1O}* (see Figure 5) are predicted to emit in the same spectral region, with predicted emission wavelengths also almost equivalent (435–444 nm), the emission of ZE^{1N}* is predicted by theory to be much more redshifted (812 nm). The former values fit very well the experimental fluorescence band at 443 nm observed in DMSO (see Figure 3 and Table 1). Given that, experimentally, this emission band presents a significant vibronic shape and that theory foresees EE* as the most stable, we attribute the 443 nm transition to the EE* form, though we cannot fully discard the possibility of having also minor contributions from the single-ESIPT KE^{1O}* form. More interestingly, theory predicts that the double-ESIPT structure in which two protons on the same side of the molecule are exchanged (KE^{2}* in Figure 5) is the most stable form in the excited-state (by -0.05 eV as compared to EE*), and its formation is therefore favoured thermodynamically. The predicted emission from the KE^{2}* state is given at 607 nm, which could fit with the low energy tail experimentally observed around 600–700 nm (see Figure 3).

One could of course wonder if triple (or even quadruple) ESIPT is not possible in **4**, and we have explored this possibility as well. Starting from KE^{2}* the two next single ESIPT are clearly uphill processes (Figure 6), and for other more exotic forms, we systematically obtain structures less stable that KE^{2}* (Figure S18, ESI†) and many with unrealistic fluorescence wavelengths, so we can safely discard the possibility of further proton transfer.

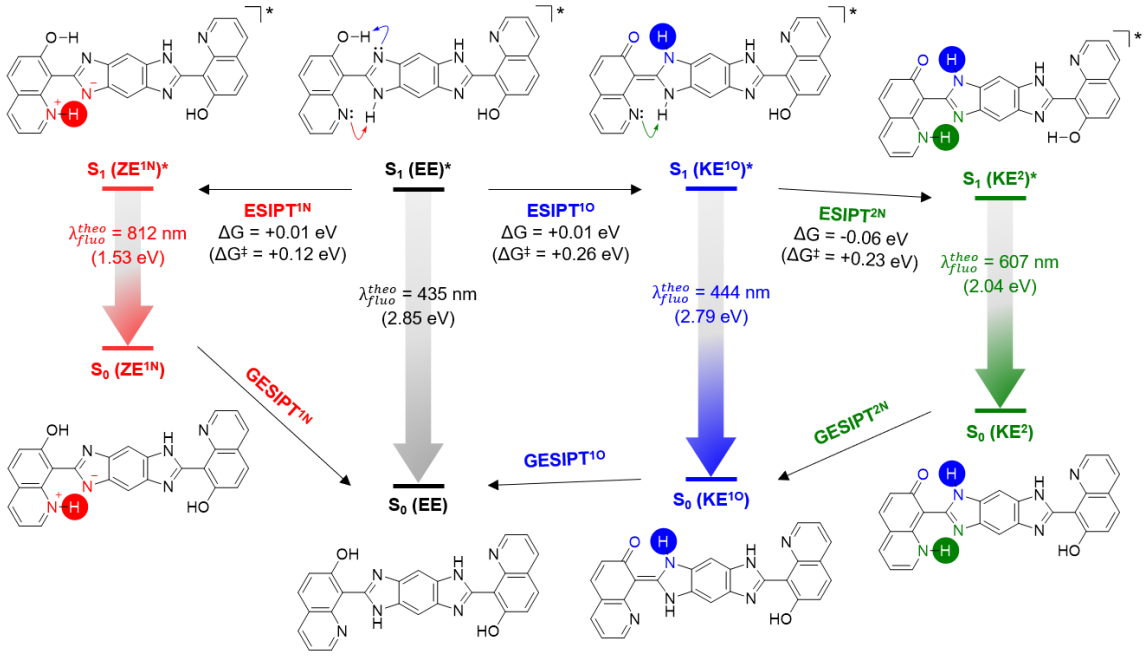

Figure 5. Computed differences of free energies (ΔG) between tautomers of **4** (1st and 2nd ESIPT) at the first excited state and computed vertical emissions (λ_{fluo}^{theo}). Level of theory: PCM-TD-TD-M06-2X/6-31G(d) for free energies, and CC2/aug-cc-pVTZ with cLR2-PCM-TD-DFT solvent corrections for wavelengths (see the ESI†). The coloured circles identify the transferred proton(s) in each tautomer. K, E and Z stand for keto, enol and zwitterionic tautomers for the two sides of each molecule. All calculations in DMSO. A scheme including additional proton transfer processes can be found Figure S18 in the ESI†.

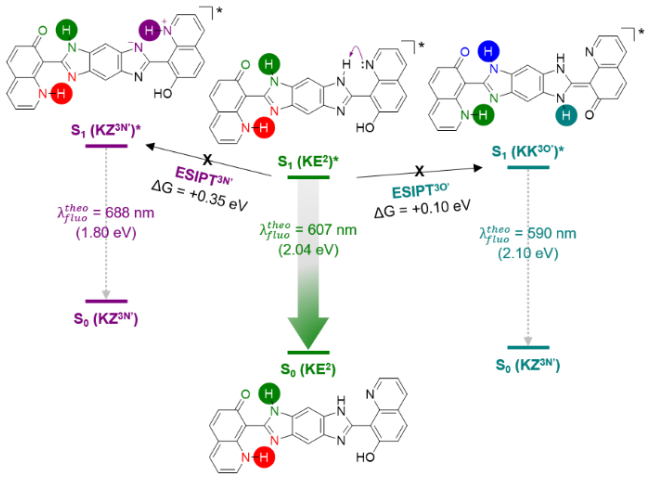

Figure 6. Computed differences of free energies (ΔG) between tautomers of **4** (3rd ESIPT) at the first excited state and computed vertical emissions (λ_{fluo}^{theo}). See caption of Figure 4 for more details.

Eventually, although as mentioned above, ESIPT is thermodynamically-driven, we have searched for the true transition state (TS) for the relevant forms displayed in Figure 5. For ESIPT^{1O} (ESIPT^{1N}) the TS is 0.26 (0.12) eV above the canonical form. The corresponding imaginary frequency if 1226*i* (1445*i*) cm^{-1}, values consistent with a PT process. These data indicate feasible ESIPT. Indeed, a simple Arrhenius equation provides an ESIPT rate of 2.5 10^8 (5.5 10^{10}) s^{-1}, competitive with emission in the ns regime (see above). It should be noted that these estimates neglect tunnelling effects and use a temperature of 298 K, *i.e.*, should be considered as lower limit of the actual rates. The ESIPT^{2N} process of Figure 5 has a TS at 0.23 eV (ν=1433*i* cm^{-1}), whereas we could not find any evidence of synchronous ESDPT, all tentative TS search corresponding to EE* to KE^2* transformation leading back to a single ESIPT case. We underline that at all TS located for the various ESIPT phenomena, a large (>0.5 eV) separation between electronic excited states pertains, while the S_1-S_0 gap remains very large (> 2 eV), so that, as stated above, there is no indication of crossings between the electronic states.

Let us now turn to **5**. As can be seen in Figure 4, the topology of the excited state is rather similar to the one of the non-substituted system, though one notes a small donating contribution from the ethynyl moieties (see Figure 4), explaining the slight redshift in the absorption spectrum. As for **4**, we have performed the same search for stable excited-state tautomers, and the key results are displayed in Figures 7 and S19 in the ESI†. In **5**, we found all structures to be less stable than the canonical EE* form by at least +0.07 eV on the free energy scale, but for KE^{1O}* that is computed to be isoenergetic with EE*. In other words, only single ESIPT could potentially take place in **5**. The computed emission wavelengths are 450 nm (EE*) and 490 nm (KE^{1O}*). By comparing the results of Figures 5 and 7, one notes that theory predicts the EE* structure to emit at nearly the same emission wavelengths (+15 nm shift only), whereas experimentally the shift is larger (+51 nm, see Figure 3). Therefore, it seems reasonable to assign the experimental fluorescence band at 495 nm to the single ESIPT KE^{1O}* structure one in **5** (computed shift of +55 nm as compared to EE* in **4**). Such assignment of the emission of **5** as resulting from single ESIPT is also consistent with the lack of vibronic structure in the experimental emission of **5**.

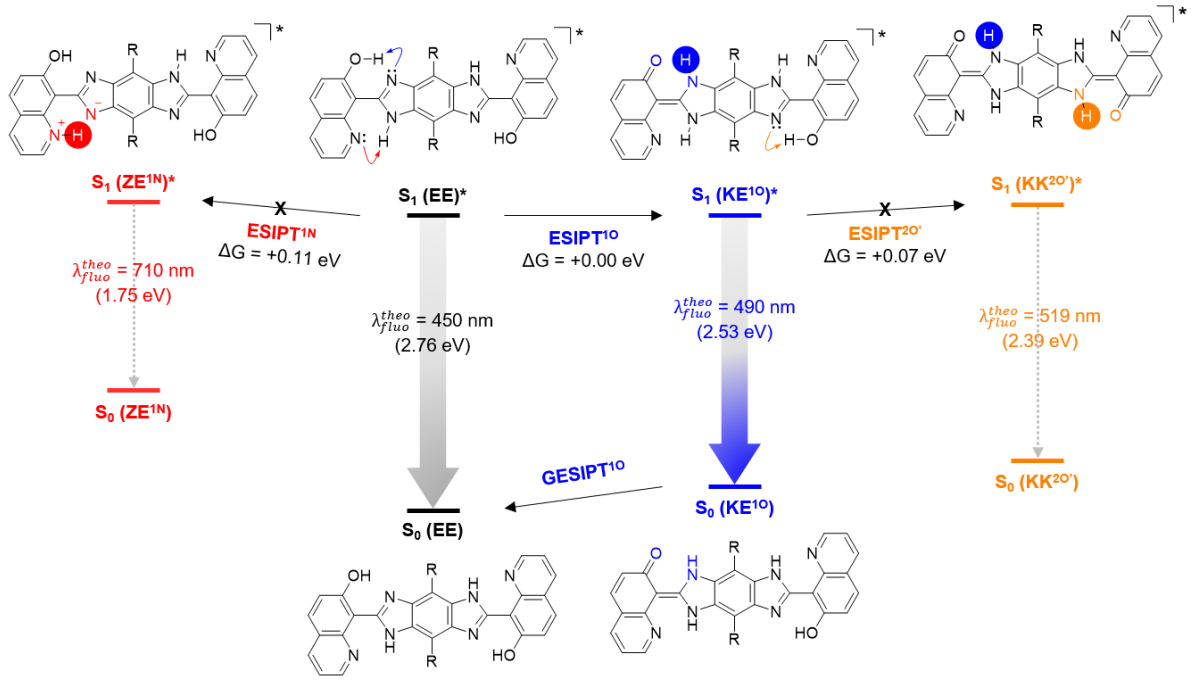

Figure 7. Computed differences of free energies (ΔG) between tautomers of **5** (R = C≡CSi(^{i}Pr$_3$)) at the first excited state and computed vertical emissions (λ_{fluo}^{theo}). The coloured circles identify the transferred proton(s) in each tautomer. K, E and Z stand for keto, enol and zwitterionic tautomers for the two sides of each molecule. All calculations in DCM. See captions of Figures 4 and 5 for more details. A scheme including additional proton transfer processes can be found Figure S19 in the ESI†.

Conclusions

In conclusion, the synthesis of novel benzobisimidazole platforms incorporating 7-hydroxyquinoline moieties and their characterization has yielded valuable insights into their photophysical properties and the potential multiple ESIPT phenomena. The absorption and emission spectra revealed redshifted optical properties and enhanced fluorescence for the ethynyl-TIPS-substituted BBI **5**, both in solution and in the solid state. Unfortunately, for both compounds, the absence of multiple emission bands in solution did not foreshadow ESDPT. These results stress that, while is it rather clear how to design systems showing single ESIPT, obtaining structures showing ESDPT is more challenging, since the first ESIPT might change the electronic structure significantly. The present study highlights the very fine balance between electronic delocalization (a too localized excited-state might prevent the second ESIPT, whereas a too delocalized one might make all proton transfer impossible), and symmetry. Theoretical calculations were essential to complement the experimental findings by predicting all the favourable single and multiple ESIPT processes with their associated emission energies. For the unsubstituted BBI **4**, the emission energies of the locally excited state and the ESIPT species are too close to be distinguished experimentally, while for the substituted BBI **5**, the emission most presumably arises for the (single) proton-transferred species. Overall, our study contributes to a deeper understanding regarding the design and properties of benzobisimidazole-based platforms for ESIPT.

Author Contributions

TM, DY and SP synthesized and characterized the compounds. TM, AG, DY and SP carried out the spectrophotometric measurements. GC carried out the electrochemical measurements. DJ performed and analysed the quantum chemical calculations. OS, AG and SP conceived the idea, designed the experiments and supervised the project. All authors critically reviewed the manuscript draft and approved the final version for submission.

Conflicts of interest

There are no conflicts to declare.

Acknowledgements

We thank the CNRS and the *ministère de* l'Enseignement *supérieur et de la Recherche* (PhD grant to T.M.). A.G. and D.Y. thank the financial support of European Union-NextGenerationEU, through the National Recovery and Resilience Plan of the Republic of Bulgaria, project № BG-RRP-2.004-0002, "BiOrgaMCT", Laboratory of Organic Functional Materials. We acknowledge the Spectropole (Aix-Marseille Univ) for HRMS analyses. D.J. is indebted to the GliCid/CCIPL computational center for allocation of computational resources.

References

1 E. D. Głowacki, M. Irimia-Vladu, S. Bauer and N. S. Sariciftci, *J. Mater. Chem. B*, 2013, **1**, 3742–3753.
2 H. R. Lee, S. A. Helquist, E. T. Kool and K. A. Johnson, *J. Biol. Chem.*, 2008, **283**, 14402–14410.
3 D. Hyatt, R. Cooke and E. Pate, *Biophys. J.*, 2009, **97**, 1952–1960.
4 Y. Itoh, Y. Nakashima, S. Tsukamoto, T. Kurohara, M. Suzuki, Y. Sakae, M. Oda, Y. Okamoto and T. Suzuki, *Sci. Rep.*, 2019, **9**, 767.
5 C. N. Pace, *Nat. Struct. Mol. Biol.*, 2009, **16**, 681–682.
6 L. R. MacGillivray and J. L. Atwood, *Nature*, 1997, **389**, 469–472.
7 X. Lin, M. Suzuki, M. Gushiken, M. Yamauchi, T. Karatsu, T. Kizaki, Y. Tani, K. Nakayama, M. Suzuki, H. Yamada, T. Kajitani, T. Fukushima, Y. Kikkawa and S. Yagai, *Sci. Rep.*, 2017, **7**, 43098.
8 A. Sikder and S. Ghosh, *Mater. Chem. Front.*, 2019, **3**, 2602–2616.
9 V. I. Tomin, A. P. Demchenko and P.-T. Chou, *J. Photochem. Photobiol. C Photochem. Rev.*, 2015, **22**, 1–18.
10 R. Plaza-Pedroche, M. P. Fernández-Liencres, S. B. Jiménez-Pulido, N. A. Illán-Cabeza, S. Achelle, A. Navarro and J. Rodríguez-López, *ACS Appl. Mater. Interfaces*, 2022, **14**, 24964–24979.
11 K. Chaihan, N. Semakul, V. Promarak, T.-T. Bui, N. Kungwan and F. Goubard, *J. Photochem. Photobiol. A*, 2022, **431**, 114047.
12 W.-S. Yu, C.-C. Cheng, Y.-M. Cheng, P.-C. Wu, Y.-H. Song, Y. Chi and P.-T. Chou, *J. Am. Chem. Soc.*, 2003, **125**, 10800–10801.
13 K. C. G. Sreedevi, A. P. Thomas, K. H. Aparna, R. Pradhan, M. L. P. Reddy, U. Lourderaj and A. Srinivasan, *Chem. Commun.*, 2014, **50**, 8667–8669.
14 X. Liu, X. Liu, Y. Shen and B. Gu, *ACS Omega*, 2020, **5**, 21684–21688.
15 K. Kanosue, T. Shimosaka, J. Wakita and S. Ando, *Macromolecules*, 2015, **48**, 1777–1785.
16 T. Stoerkler, T. Pariat, A. D. Laurent, D. Jacquemin, G. Ulrich and J. Massue, *Molecules*, 2022, **27**, 2443.
17 Y. Yang, Y. Ding, W. Shi, F. Ma and Y. Li, *J. Lumin.*, 2020, **218**, 116836.
18 T. Pariat, M. Munch, M. Durko-Maciag, J. Mysliwiec, P. Retailleau, P. M. Vérité, D. Jacquemin, J. Massue and G. Ulrich, *Chem. Eur. J*, 2021, **27**, 3483–3495.
19 G. Zhao, W. Shi, X. Xin, F. Ma and Y. Li, *J. Mol. Liq.*, 2022, **354**, 118807.
20 C. Balakrishnan, M. A. Neelakantan and S. Banerjee, *Sens. Actuators B Chem.*, 2017, **253**, 1012–1025.
21 Y. Li, D. Dahal, C. S. Abeywickrama and Y. Pang, *ACS Omega*, 2021, **6**, 6547–6553.
22 N. A. Shekhovtsov, E. B. Nikolaenkova, A. S. Berezin, V. F. Plyusnin, K. A. Vinogradova, D. Yu. Naumov, N. V. Pervukhina, A. Ya. Tikhonov and M. B. Bushuev, *Dalton Trans.*, 2022, **51**, 15166–15188.
23 N. A. Shekhovtsov, K. A. Vinogradova, S. N. Vorobyova, A. S. Berezin, V. F. Plyusnin, D. Yu. Naumov, N. V. Pervukhina, E. B. Nikolaenkova, A. Ya. Tikhonov and M. B. Bushuev, *Dalton Trans.*, 2022, **51**, 9818–9835.
24 J. Guan, Q. Tu, L. Chen, M.-S. Yuan and J. Wang, *Spectrochim. Acta. A. Mol. Biomol. Spectrosc.*, 2019, **220**, 117114.
25 M. Mathivanan, B. Tharmalingam, C.-H. Lin, B. V. Pandiyan, V. Thiagarajan and B. Murugesapandian, *CrystEngComm*, 2020, **22**, 213–228.
26 P. Zhou and K. Han, *Aggregate*, 2022, **3**, e160.

27 V. S. Padalkar and S. Seki, *Chem. Soc. Rev.*, 2016, **45**, 169–202.
28 L. Chen, P.-Y. Fu, H.-P. Wang and M. Pan, *Adv. Opt. Mater.*, 2021, **9**, 2001952.
29 L. G. T. A. Duarte, J. C. Germino, J. F. Berbigier, C. A. Barboza, M. M. Faleiros, D. de Alencar Simoni, M. T. Galante, M. S. de Holanda, F. S. Rodembusch and T. D. Z. Atvars, *Phys. Chem. Chem. Phys.*, 2019, **21**, 1172–1182.
30 K. Wang, R. Hu, J. Wang, J. Zhang, J. Liu, L. Zhou, L. Zhou and B. Li, *ACS Materials Lett.*, 2022, **4**, 2337–2344.
31 K. Wang, L. Wan, J. Wang, C. Zhou, K. Yang, L. Zhou and B. Li, *Chin. Chem. Lett.*, 2024, 35, 109554.
32 M. Durko-Maciag, G. Ulrich, D. Jacquemin, J. Mysliwiec and J. Massue, *Phys. Chem. Chem. Phys.*, 2023, **25**, 15085–15098.
33 B. Blagoeva, A. Stoilova, D. Dimov, D. Yordanov, D. Nazarova, A. Georgiev and L. Antonov, *Photochem. Photobiol. Sci.*, 2021, **20**, 687–697.
34 J. Zhao, S. Ji, Y. Chen, H. Guo and P. Yang, *Phys. Chem. Chem. Phys.*, 2012, **14**, 8803–8817.
35 M. Jadhao, O. R. Meitei, R. Joshi, H. Kumar, C. Das and S. K. Ghosh, *J. Photochem. Photobiol. Chem.*, 2016, **326**, 41–49.
36 Q. Chen, C. Jia, Y. Zhang, W. Du, Y. Wang, Y. Huang, Q. Yang and Q. Zhang, *J. Mater. Chem. B*, 2017, **5**, 7736–7742.
37 S. Hu, J. Wang, M. Luo, Z. Wu, Y. Hou and X. Chen, *Anal. Bioanal. Chem.*, 2021, **413**, 5463–5468.
38 K. Stock, C. Schriever, S. Lochbrunner and E. Riedle, *Electron Correl. Mol. Dyn. Excit. States Photochem.*, 2008, **349**, 197–203.
39 F. Plasser, M. Barbatti, A. J. A. Aquino and H. Lischka, *J. Phys. Chem. A*, 2009, **113**, 8490–8499.
40 Y. Hao and Y. Chen, *Dyes Pigments*, 2016, **129**, 186–190.
41 J. Zhao and Y. Zheng, *Sci. Rep.*, 2017, **7**, 44897.
42 I. E. Serdiuk and A. D. Roshal, *Dyes Pigments*, 2017, **138**, 223–244.
43 J. Zhao, H. Dong and Y. Zheng, *J. Phys. Chem. A*, 2018, **122**, 1200–1208.
44 J. Massue, D. Jacquemin and G. Ulrich, *Chem. Lett.*, 2018, **47**, 1083–1089.
45 P. M. Vérité, C. A. Guido and D. Jacquemin, *Phys. Chem. Chem. Phys.*, 2019, **21**, 2307–2317.
46 J. Zhao, Y. Yang, L. Li and H. Zhang, *ChemistrySelect*, 2023, **8**, e202301202.
47 T. Wróblewski and D. Ushakou, *J. Fluoresc.*, 2023, **33**, 103–111.
48 D. De, K. Santra and A. Datta, *J. Phys. Chem. B*, 2012, **116**, 11466–11472.
49 J. Sepioł, H. Bulska and A. Grabowska, *Chem. Phys. Lett.*, 1987, **140**, 607–610.
50 O. K. Abou-Zied, *J. Photochem. Photobiol. A*, 2006, **182**, 192–201.
51 H. Lim, S.-Y. Park and D.-J. Jang, *J. Phys. Chem. A*, 2010, **114**, 11432–11435.
52 K.-C. Tang, C.-L. Chen, H.-H. Chuang, J.-L. Chen, Y.-J. Chen, Y.-C. Lin, J.-Y. Shen, W.-P. Hu and P.-T. Chou, *J. Phys. Chem. Lett.*, 2011, **2**, 3063–3068.
53 Y. Liu, Y. Yang, X. Jia, Q. Ma, Y. He, H. Zhai, Y. Zhang and Y. Liu, *J. Mol. Liq.*, 2020, **302**, 112552.
54 G. Kumar, K. Paul and V. Luxami, *New J. Chem.*, 2020, **44**, 12866–12874.
55 M. Tasior, V. Hugues, M. Blanchard-Desce and D. T. Gryko, *Chem. Asian J.*, 2012, **7**, 2656–2661.
56 E. A. Shilova, A. Heyndericкx and O. Siri, *J. Org. Chem.*, 2010, **75**, 1855–1861.
57 C. Azarias, Š. Budzák, A. D. Laurent, G. Ulrich and D. Jacquemin, *Chem. Sci.*, 2016, **7**, 3763–3774.
58 M. Raoui, J. Massue, C. Azarias, D. Jacquemin and G. Ulrich, *Chem. Commun.*, 2016, **52**, 9216–9219.